Jordan Journal of Civil Engineering, Volume **18**, No. **3**, **2024**
DOI: https://doi.org/10.14525/JJCE.v18i3.05

Jordan Journal of Civil Engineering

Journal homepage: https://jjce.just.edu.jo

Seismic Responses of Large Height-Width Ratio Liquid Storage Structure with Base Isolation and Baffles

Wei Jing [1,2]* ***and Yixin Zhang*** [1]

[1] *Western Engineering Research Center of Disaster Mitigation in Civil Engineering of Ministry of Education, Lanzhou University of Technology, Lanzhou, 730050, PR China. * Corresponding Author. E-Mail: jingwei3276@163.com*

[2] *Key Laboratory of Earthquake Engineering and Engineering Vibration, Institute of Engineering Mechanics, China Earthquake Administration.*

ARTICLE INFO

Article History:
Received: 15/8/2023
Accepted: 9/5/2024

ABSTRACT

With the shortage of land resources, the engineering application of large height-width ratio liquid storage structure is of great significance. 3-D numerical calculation models of large height-width ratio liquid storage structure are established by ANSYS. The elements Solid 65 and Solid 185 are used to simulate the concrete and the bearing, while the element Fluid 80 is used to simulate the liquid. The dynamic responses of four types of structure are comparatively investigated, which are non-isolated structure with double baffles, isolated structure with double baffles, non-isolated structure with triple baffles and isolated structure with triple baffles. The results show that under the Tianjin waves, the wall tensile stress of the non-isolated structure with triple baffles is decreased by 50% compared to the non-isolated structure with double baffles, while the wall tensile stresses of the isolated structures with double and triple baffles are increased by 10% and 122%, respectively, compared to those of the non-isolated structures. It is shown that conventional rubber isolation is not suitable for the large height-width ratio liquid storage structures with baffles, where the load-bearing capacity and safety of the structure can be improved by increasing the number of horizontal baffles.

Keywords: Liquid storage structure, Base isolation, Shock absorption, Fluid-structure interaction, Dynamic response.

INTRODUCTION

Concrete rectangular liquid storage structure is widely used, while the traditional concrete liquid storage structures are mostly low structures, which makes them occupy a large amount of land resources. With the development of cities and the shortage of land resources, it is necessary to conduct theoretical and engineering application research of concrete liquid storage structures with large height-width ratio without influencing the liquid storage capacity. The seismic damage of the liquid storage structure will not only lead to the abnormal operation of the whole system, but also to other secondary disasters. There were many cases of concrete liquid storage structure damage in previous earthquakes; for example, in September 1923, an earthquake of magnitude 7.9 occurred in Kanto, Japan and most of liquid storage structures collapsed or cracked. In

February 1975, most of the liquid storage structures were irreparably damaged in the Haicheng earthquake of magnitude 7.3 in Liaoning province, China. An earthquake of magnitude 8.0 occurred in Wenchuan on May 12, 2008 and caused almost irreparable damage to the liquid storage structures in the extreme earthquake zone. In April 2010, two high level liquid storage structures were damaged in the Yushu earthquake of magnitude 7.1 in Qinghai province, China. As the concrete liquid storage structure with large height-width ratio has just entered the stage of popularization and application, there is a lack of necessary statistical data of earthquake damage. It is necessary to realize the reasonable design of this kind of structure by theoretical, numerical simulation and experimental methods and promote its engineering application.

Many studies on the base-isolated liquid storage tank have been carried out. Luo et al. (2016) developed a hybrid control system by combination of viscous mass damper (VMD) and rubber bearing and observed that the sloshing heights of the liquid base sheared, with overturning moments of the tanks being reduced through the application of the proposed method. Safari and Tarinejad (2018) investigated seismic response of base isolated steel liquid storage tanks by a stochastic approach in frequency domain and concluded that the sloshing response of the tanks is significantly reduced by sliding bearing. Saha et al. (2016) investigated the influence of input parameter uncertainty on peak response quantities and fragility curves of base-isolated liquid storage tanks and concluded that when the uncertainties in the input parameters increased, the probability of failure at a given amplitude of excitation was also increased. Nikoomanesh et al. (2019) proposed a new vertical seismic isolation of an aboveground liquid storage tank and concluded that the overturning moment of the tanks equipped with the proposed isolation system decreased significantly with respect to the corresponding fully anchored tanks. Rawat et al. (2019) carried out a numerical study of the base-isolated ground-supported cylindrical liquid storage tank using the finite element method and obtained that as the time period of the isolator increased; i.e., increased flexibility, the base shear response was considerably reduced in both rigid and flexible, broad and slender tanks. Tang et al. (2021) conducted a real-time hybrid simulation to compare the seismic performance of the storage tanks isolated by friction pendulum bearing (FPB), laminated rubber bearing (LRB) and variable curvature friction pendulum bearing (VCFPB) and concluded that the low-frequency components of shear force and overturning moment were amplified by LRB. In contrast, the FPB and VCFPB had a good performance on all frequency bands.

The main characteristic of the concrete rectangular liquid storage structure with large height-width ratio is that with the increase of liquid storage height, the liquid pressure acting on the wall also increases. It is necessary to find a strengthening method. This paper attempts to introduce the method of adding horizontal baffles with holes to reduce the pressure acting on the wall. Baffles are widely used in low liquid storage structures and a series of studies have been carried out on the liquid storage structure with baffles. Cheng et al. (2019) derived the simplified calculation method of the dynamic liquid pressure acting on the vertical baffle of liquid storage tank and concluded that the farther the baffle is deviated from the central axis of the liquid storage tank, the larger the dynamic liquid pressure. Hosseini et al. (2019) proposed a passive control technique that reduced the maximum sloshing height by using a Suspended Annular Baffle (SAB) and concluded that using a SAB reduced the maximum seismic sloshing height, in average, to a value between 80% and 40% of its value in the non-baffled case. Zang et al. (2019) studied the effects of the porous baffle length, porosity and design on the sloshing force, wave surface elevation and velocity field. Hajimehrabi et al. (2019) concluded that the baffle significantly decreased the sloshing wave height by (11%-67%), but resulted in an increase of about 10% in the vertical crack width and the base bending moment of the tank wall. Sun et al. (2020) discussed the effects of the baffle position and size on the dynamic behavior of a tank-liquid system. Jin et al. (2021) examined the damping baffle effect on the pressure response under impulsive and convective modes and developed a suitable damping baffle system for the liquid storage tank.

It is also of great significance to combine the isolation with baffle and carry out its application research in the liquid storage structure. Cheng et al. (2018) arranged vertical baffles into a base-isolated concrete liquid storage structure and improved the energy dissipation by opening holes in the baffles. Shekari et al. (2019) analyzed the simultaneous influences of base-isolator system and vertical baffles on the seismic performance of a three-dimensional (3D) rectangular liquid storage tank and concluded that baffles reduced the peak base moment response by as high as 19% on average compared with the fixed-base slender tank without baffles. Rawat and Matsagar (2022) analyzed liquid storage tanks using the coupled acoustic-structural approach in the finite element method and observed that the oblate spheroid base isolation system was efficient in mitigating the seismic responses in the tanks and the surface diaphragm was efficient in controlling the sloshing displacement.

The application of concrete liquid storage structure with a large aspect ratio is helpful to save land resources. A great deal of research has been carried out on the seismic dynamic responses of traditional low concrete liquid storage structures and the existing research can provide a theoretical basis for the study of liquid storage structures. It is of great significance to study the engineering application of concrete rectangular liquid storage structure with large height-width ratio, but the main feature of the concrete rectangular liquid storage structure with large height-width ratio is that the liquid pressure on the wall increases with the increase of the liquid storage height, which can easily lead to cracking and failure of the wall under the action of earthquake. In this paper, considering fluid-structure interaction and material nonlinearity, a 3-D numerical calculation model of large height-width ratio liquid storage tanks with isolation and horizontal baffle is established based on the finite element method. The seismic control effect on concrete rectangular liquid storage structure with large height-width ratio is discussed, thus providing a reference for the engineering application of this kind of structure.

DYNAMIC EQUATIONS

The classical Navier-Stokes equation can describe the dynamic behavior of liquid, for incompressible Newtonian fluids, where the momentum equation has the following form (Shekari et al., 2019):

$$\begin{cases} \rho_f \dfrac{\partial v_f}{\partial t} + \rho_f\left[\left(v_f - \bar{v}_f\right)\cdot \nabla\right] v_f = \nabla \cdot \tau + f^B \\ \dfrac{\partial \rho_f}{\partial t} + \left(v_f - \bar{v}_f\right)\cdot \nabla \rho_f + \rho_f \nabla \cdot v_f = 0 \\ \rho_f \dfrac{\partial E}{\partial t} + \rho_f\left(v_f - \bar{v}_f\right)\cdot \nabla E = \tau_f \cdot D - \nabla \cdot q + q^B \end{cases} \quad (1)$$

where ρ_f is the liquid density; v_f is the liquid velocity; $\bar{v}_f$ is the coordinate system velocity; τ_f is the liquid stress tensor; f^B is the external force vector acting on the liquid; E is the specific internal energy; *and* D is the strain rate tensor.

When the liquid interacts with a solid medium, equilibrium and compatibility equations must be satisfied on the contact surface (Rawat and Matsagar, 2022):

$$\begin{cases} \tau^s \cdot \boldsymbol{n} = \tau^f \cdot \boldsymbol{n} \\ u_s^I = u_f^I \\ v_s^I = v_f^I = \bar{v}_f^I \\ a_s^I = a_f^I = \bar{a}_f^I \end{cases} \quad (2)$$

where $\boldsymbol{n}$ is the normal vector on the contact surface; u_s and u_f are the structure and liquid displacements on the contact surface; v_s, v_f and $\bar{v}_f$ are the structure, liquid and coordinate system velocities; a_s, a_f and $\bar{a}_f$ are the structure, liquid and coordinate system accelerations; and I represents the contact surface.

The relationship between liquid pressure and volumetric strain is as follows (Sun et al., 2020):

$$\begin{Bmatrix} P \\ P_x \\ P_y \\ P_z \end{Bmatrix} = \begin{bmatrix} C_{11} & & & \\ & C_{22} & & \\ & & C_{33} & \\ & & & C_{44} \end{bmatrix} \begin{Bmatrix} \varepsilon_v \\ w_x \\ w_y \\ w_z \end{Bmatrix} \quad (3)$$

where P is the liquid pressure; C_{11} is the bulk modulus; P_x, P_y and P_z are the rotational stresses; C_{22}, C_{33} and C_{44} are the constraint parameters; w_x, w_y and w_z are the rotations about the Cartesian axes x, y and z, respectively, and ε_v is the volumetric strain. The specific formulae are shown in Appendix A.

u_{fx}, u_{fy} and u_{fz} are the displacement components of liquid in x, y and z directions.

By using the finite element method, the liquid strain energy, free liquid surface potential energy and liquid kinetic energy can be expressed as (Sun et al., 2020):

$$\Pi_e = \frac{1}{2}\boldsymbol{u}_f^T\boldsymbol{K}_f\boldsymbol{u}_f \qquad (4)$$

$$\Pi_s = \frac{1}{2}\boldsymbol{u}_{fs}^T\boldsymbol{S}_f\boldsymbol{u}_{fs} \qquad (5)$$

$$T = \frac{1}{2}\dot{\boldsymbol{u}}_f^T\boldsymbol{M}_f\boldsymbol{u}_f \qquad (6)$$

where $\mathbf{S}_f$ and $\mathbf{u}_{fs}$ are the free surface stiffness matrix and free surface vertical displacement vector, $\mathbf{K}_f$ and $\mathbf{M}_f$ are the stiffness and mass matrices of the liquid, respectively. The specific formulae are shown in Appendix A.

According to the virtual work principle, the interaction boundary of a three-dimensional element should be expressed as (Avval 2012):

$$\int \boldsymbol{P}^e\boldsymbol{u}_n^e\,ds = \boldsymbol{f}_e^T\boldsymbol{\delta} = \begin{bmatrix} f_{x1} & f_{y1} & f_{z1} & f_{x2} & f_{y2} & f_{z2}\end{bmatrix} \begin{bmatrix} u_1 & v_1 & w_1 & u_2 & v_2 & w_2\end{bmatrix}^T \qquad (7)$$

where $\boldsymbol{P}^e$ and $\boldsymbol{u}_n^e$ are the pressure and normal displacement along the element interface; $\boldsymbol{f}_e$ is the force acting on the element; $\boldsymbol{\delta}$ is the element displacement; f_x, f_y and f_z are the node forces in the *x*, *y* and *z* directions; *u*, *v* and *w* are the node displacements in the *x*, *y* and *z* directions; *and e* represents the element on the interaction boundary.

The dynamic equation of the structure can be expressed as:

$$\boldsymbol{M}_s\ddot{\boldsymbol{u}}_s(t) + \boldsymbol{C}_s\dot{\boldsymbol{u}}_s(t) + \boldsymbol{K}_s\boldsymbol{u}_s(t) = -\boldsymbol{M}_s\ddot{\boldsymbol{u}}_g(t) + \boldsymbol{QP} \qquad (8)$$

where $\mathbf{M}_s$, $\mathbf{C}_s$ and $\mathbf{K}_s$ are the positive definite n×n order mass, damping and stiffness matrices, respectively; $\boldsymbol{u}_s(t)$, $\dot{\boldsymbol{u}}_s(t)$ and $\ddot{\boldsymbol{u}}_s(t)$ are the displacement, velocity and acceleration vectors of the coupled system; $\ddot{\boldsymbol{u}}_g(t)$ is the earthquake acceleration vector; $\boldsymbol{Q}$ is the fluid-structure coupling matrix; and $\boldsymbol{P}$ is the hydrodynamic pressure.

Assuming that $\boldsymbol{F}_1 = -\boldsymbol{M}\ddot{\boldsymbol{u}}_g(t)$, then Eq. (8) is further simplified as:

$$\boldsymbol{M}_s\ddot{\boldsymbol{u}}(t) + \boldsymbol{C}_s\dot{\boldsymbol{u}}(t) + \boldsymbol{K}_s\boldsymbol{u}(t) = \boldsymbol{F}_1 + \boldsymbol{QP} \qquad (9)$$

Considering the great difference in damping between the rubber, the liquid and the structure, the material dependent damping is applied in the model (Cai et al., 2002). The form of the damping matrix **C** is shown in Appendix A.

In the liquid domain, the motion equation of the boundary element can be expressed as (Cheng et al., 2018):

$$\boldsymbol{G}\ddot{\boldsymbol{P}} + \boldsymbol{C}'\dot{\boldsymbol{P}} + \boldsymbol{HP} = -\rho_f\boldsymbol{Q}^T(\ddot{\boldsymbol{u}}_s + \ddot{\boldsymbol{u}}_g) \qquad (10)$$

Assuming that $\boldsymbol{F}_2 = -\rho_f\boldsymbol{Q}^T\ddot{\boldsymbol{u}}_g$, then Eq. (10) is further simplified as:

$$\boldsymbol{G}\ddot{\boldsymbol{P}} + \boldsymbol{C}'\dot{\boldsymbol{P}} + \boldsymbol{HP} = \boldsymbol{F}_2 - \rho_f\boldsymbol{Q}^T\ddot{\boldsymbol{u}}_s \qquad (11)$$

Based on the above structure and liquid equations, the dynamic equation of liquid-solid coupling system in time domain can be obtained as:

$$\begin{bmatrix} \boldsymbol{M}_s & 0 \\ \rho_f\boldsymbol{Q}^T & \boldsymbol{G}\end{bmatrix}\begin{Bmatrix}\ddot{\boldsymbol{u}}_s \\ \ddot{\boldsymbol{P}}\end{Bmatrix} + \begin{bmatrix} \boldsymbol{C}_s & 0 \\ 0 & \boldsymbol{C}'\end{bmatrix}\begin{Bmatrix}\dot{\boldsymbol{u}}_s \\ \dot{\boldsymbol{P}}\end{Bmatrix} + \begin{bmatrix} \boldsymbol{K}_s & -\boldsymbol{Q} \\ 0 & \boldsymbol{H}\end{bmatrix}\begin{Bmatrix}\boldsymbol{u}_s \\ \boldsymbol{P}\end{Bmatrix} = \begin{Bmatrix}\boldsymbol{F}_1 \\ \boldsymbol{F}_2\end{Bmatrix} \qquad (12)$$

NUMERICAL EXAMPLE

Calculation Model

The modulus of elasticity of concrete is 3×10^{10}Pa, the Poisson's ratio is 0.2, the shear transfer coefficient for open crack and closed crack are 0.5 and 0.95, respectively (Shakir and Hamad, 2021). The uniaxial tensile cracking stress is 2.39MPa and the multi-linear isotropic model is used for the concrete. The elements Solid 65 and Solid 185 are used to simulate the concrete and the bearing, while the element Fluid 80 is used to simulate the liquid. Solid 65 is defined by eight nodes having three degrees of freedom at each node, with translations in the *x*, *y* and *z* directions (Shakir and Kamonna 2016; Shakir and Abdlsaheb, 2022). Fluid 80 has 8 nodes, each node has 3 degrees of freedom, with translational motion in the *x*, *y* and *z* directions (Cheng et al., 2018). Solid 185 is defined by eight nodes having three degrees of freedom at each node, with translations in the *x*, *y* and *z* directions (Shakir, 2016; Shakir and Al-Sahlawi, 2023). The main materials and elements for the model are shown in Table A1 in appendix A. The liquid depth is 8.6m and the springs are placed on the liquid free surface to simulate the restoring force effect of the fluid under the action of gravity. The size of the rubber isolation bearing is 0.3 m×0.3 m×0.2 m and the number of the bearing is 9. The coupling degree of freedom is used to deal with the relationship between the structure and the liquid. The method of coupling degrees of freedom is used to deal with the relationship between the tank wall, the tank bottom and the liquid. The cpintf, u*x* (u*y*) is used to deal with the overlap node between the tank wall and the liquid and the cpintf, u*z* is used to deal with the overlap node between the tank bottom and the liquid. The near-field El-Centro waves and the far-field Tianjin waves are selected and PGA is amplitude-modulated to 0.2g, 0.4g and 0.6g for dynamic time history analysis. The geometric parameters of the concrete rectangular liquid storage tank are shown in Fig. 1. The finite element models with double baffles and triple baffles are shown in Fig. 2 and Fig. 3, respectively. The acceleration time history curves of the seismic waves are shown in Fig. 4.

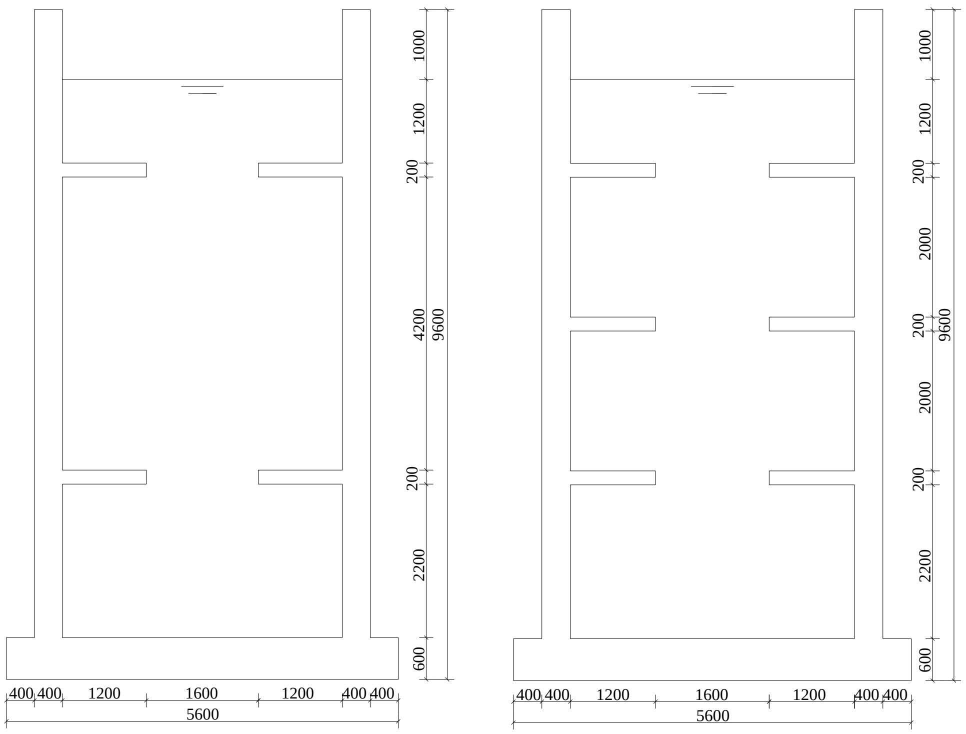

(a) Structure with double baffles (b) Structure with triple baffles

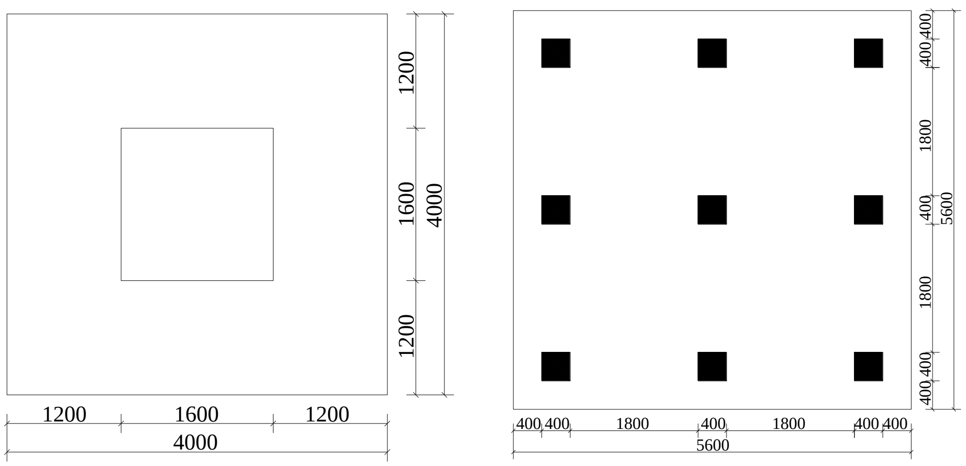

(c) Baffle (d) Rubber bearing arrangement

Figure (1): Geometric information (unit: mm)

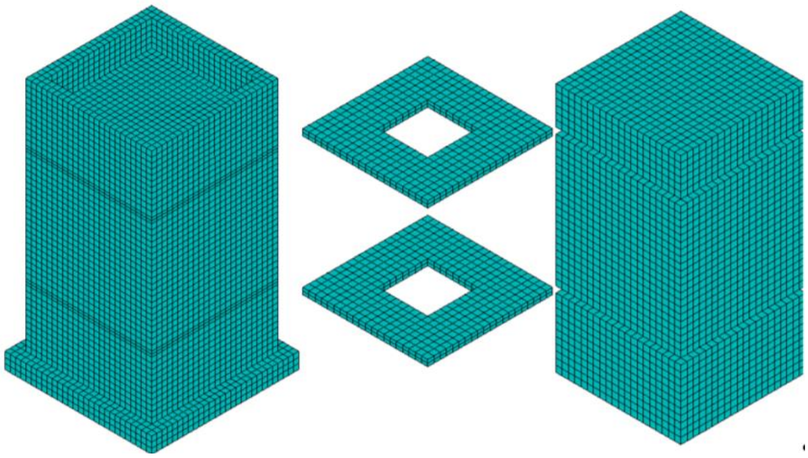

(a) Whole model (b) Baffles (c) Liquid

Figure (2): Calculation model of structure with double baffles

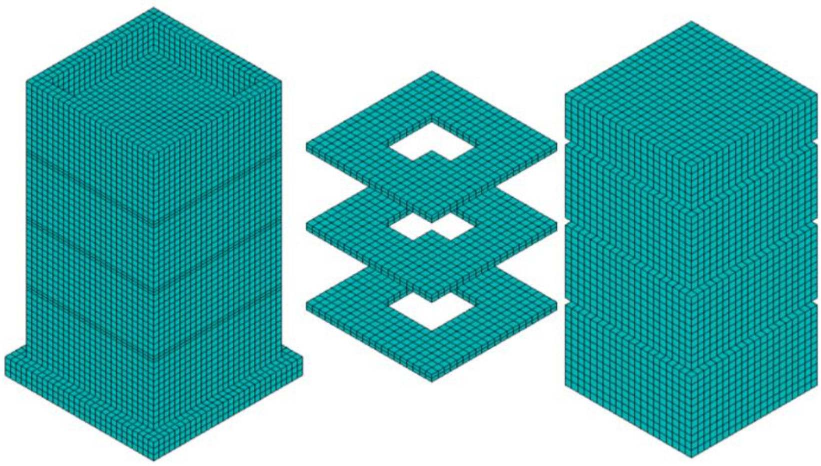

(a) Whole model (b) Baffles (c) Liquid

Figure (3): Calculation model of structure with triple baffles

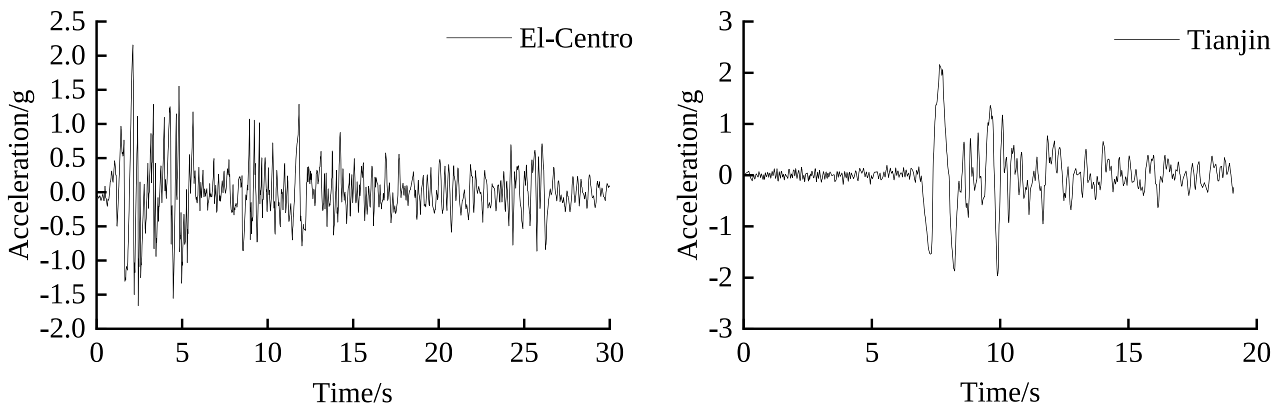

Figure (4): Seismic waves

The rubber isolation bearing is simulated by the Mooney-Rivlin two-parameter material model and its elastic strain energy function W is as follows:

$$W = C_{10}(I_1 - 3) + C_{01}(I_2 - 3) + \frac{1}{D_1}(J - 1)^2 \qquad (13)$$

where C_{10} and C_{01} are the material constants generally determined by the experiment (Jianlong et al., 2008); I_1 and I_2 are the first and the second invariants of the deviatoric component of the Cauchy-Green deformation tensor. D_1 is the incompressibility coefficient and J is the ratio of the deformation volume to the undeformed volume.

Initial shear modulus G_0 and initial Young's modulus E_0 can be expressed as follows (Sussman & Bathe, 1987):

$$G_0 = 2(C_{10} + C_{01}) \tag{14}$$

$$E_0 = 3G_0 \tag{15}$$

Modal Analysis

The Lanczos method and the reduction method are used for the modal calculation and analysis of the structure and the liquid, respectively. The first and the second modes of the structure and the liquid corresponding to double baffles and triple baffles are shown in Figs. 5-8, respectively. It is shown that the number of baffles is increased from 2 to 3 and the structure and liquid vibration frequency are less affected.

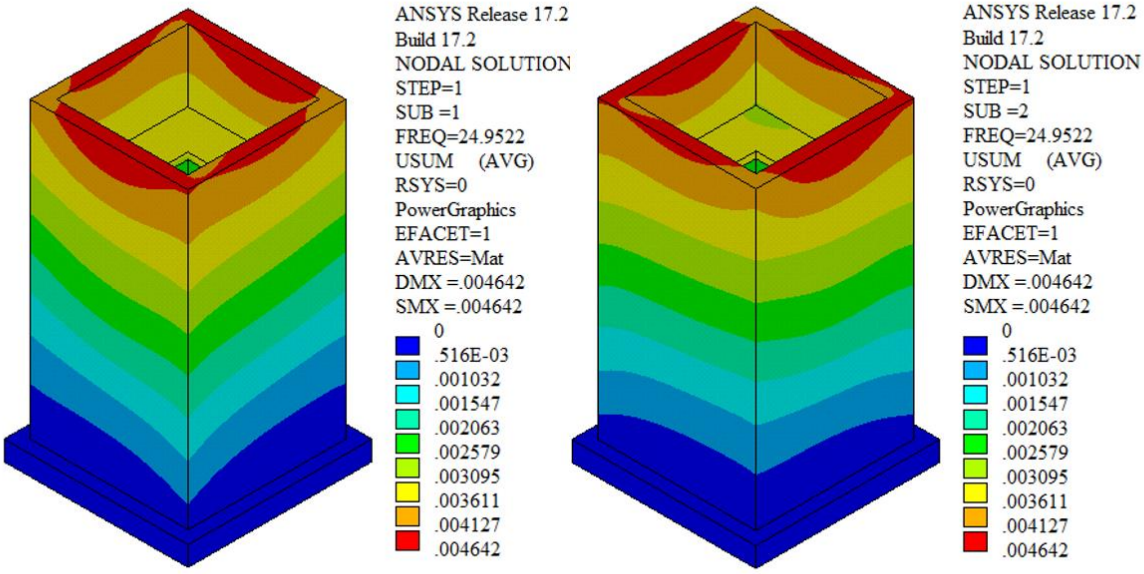

(a) First mode (b) Second mode

Figure (5): Modes of structure with double baffles

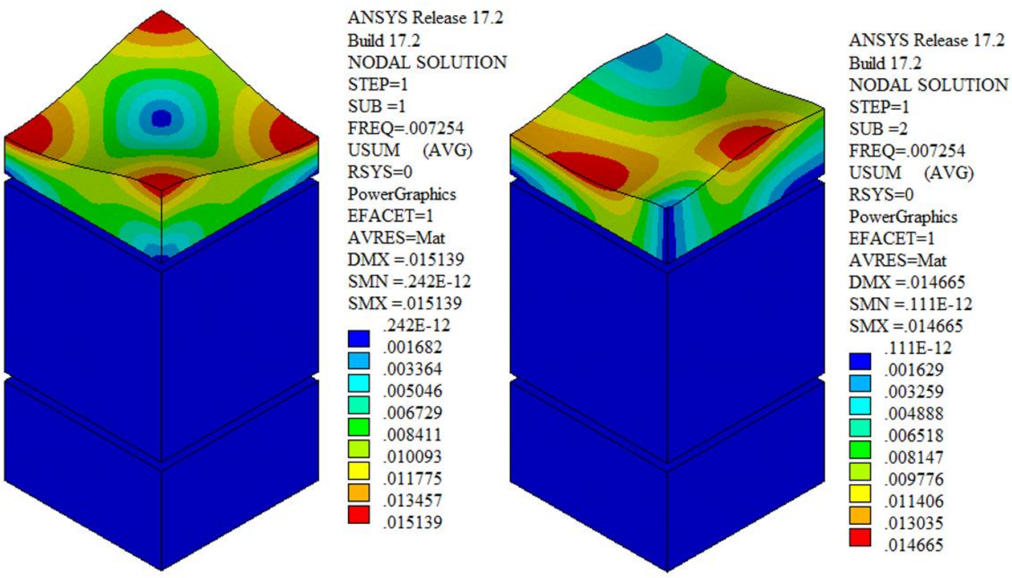

(a) First mode (b) Second mode

Figure (6): Modes of liquid corresponding to double baffles

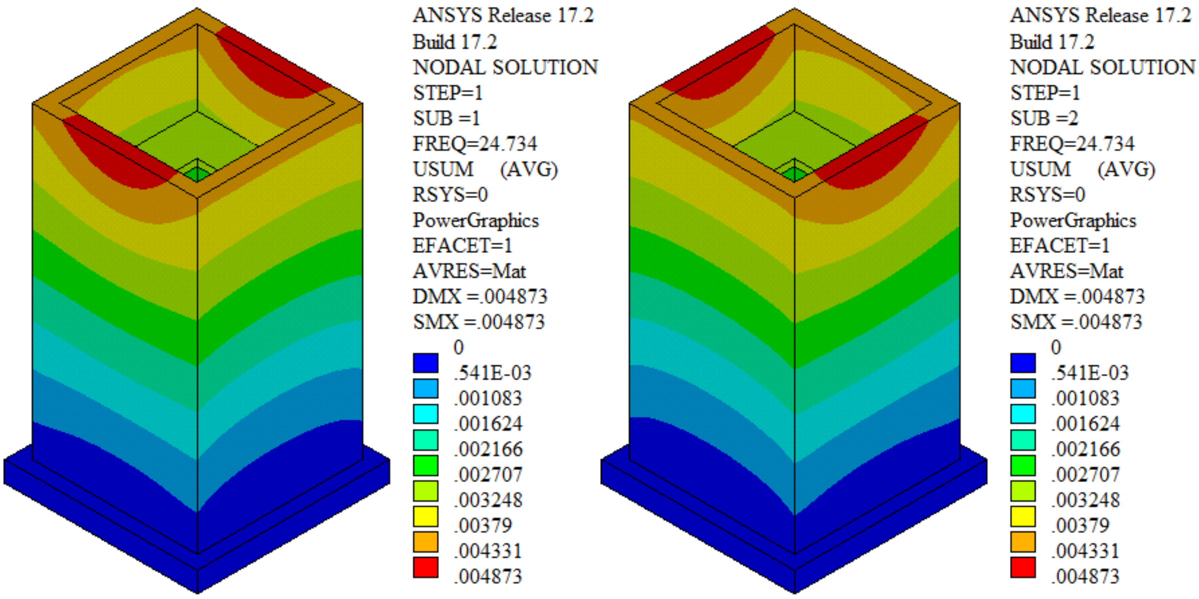

(a) First mode (b) Second mode

Figure (7): Modes of structure with triple baffles

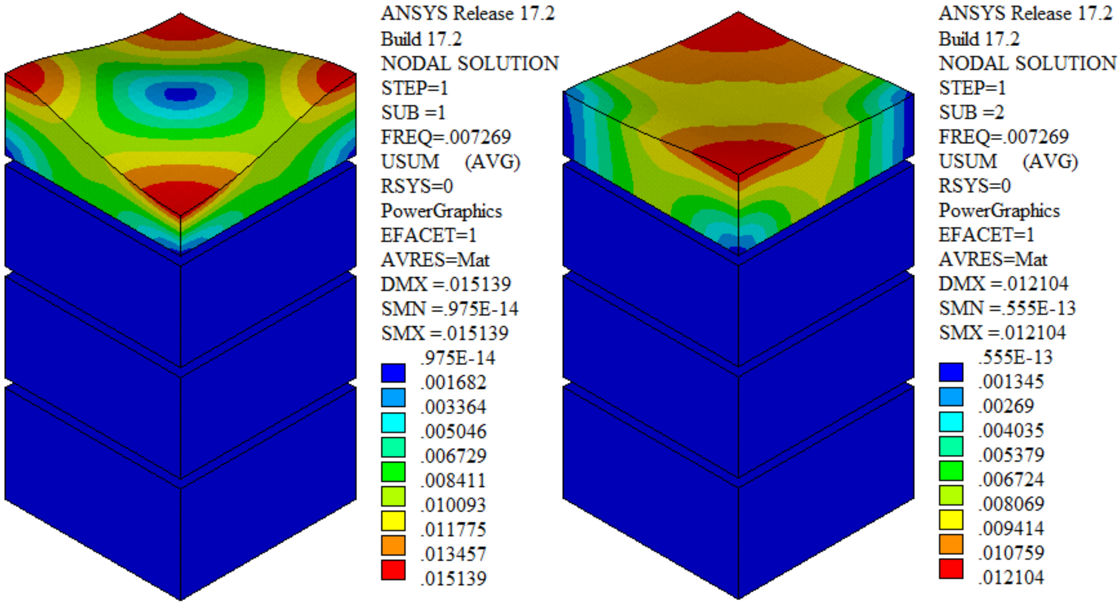

(a) First mode (b) Second mode

Figure (8): Modes of liquid corresponding to triple baffles

Dynamic Responses

In order to study the damping control effect of the rubber isolation and horizontal baffle on the concrete rectangular liquid storage structures with large height-width ratio and the seismic dynamic responses of structures with different numbers of horizontal baffles and with or without rubber isolation are calculated, respectively.

Tensile Stress

For the concrete structure, the tensile stress is an important dynamic response under earthquake and the wall cracking is one of the main failure modes of concrete liquid storage structures. Due to space limitations, taking El-Centro waves (PAG=0.4g) as an example, the nephograms of wall plate and baffles are shown in Fig. 9 and Fig. 11. The calculation results of tensile stress of wall plate and baffles corresponding to PGA of 0.2g, 0.4g and 0.6g are shown in Fig. 10 and Fig. 12.

(1) Wall stress

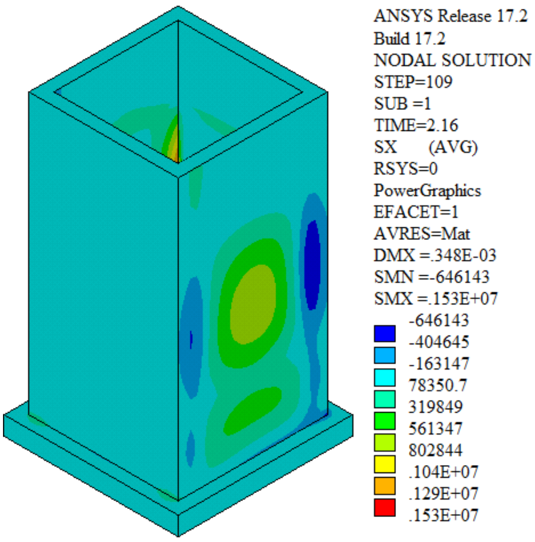

(a) Non-isolated structure with double baffles

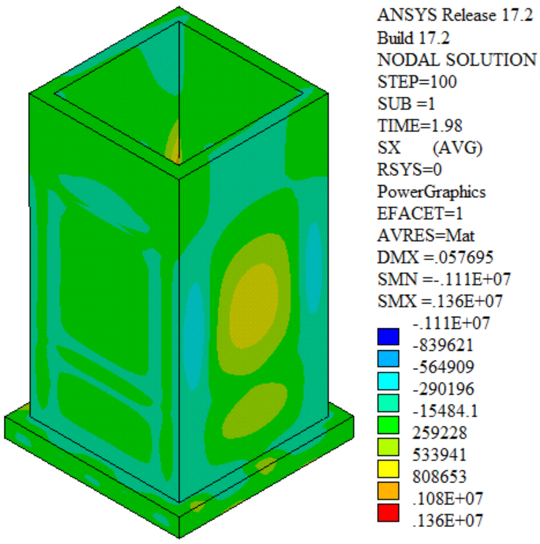

(b) Isolated structure with double baffles

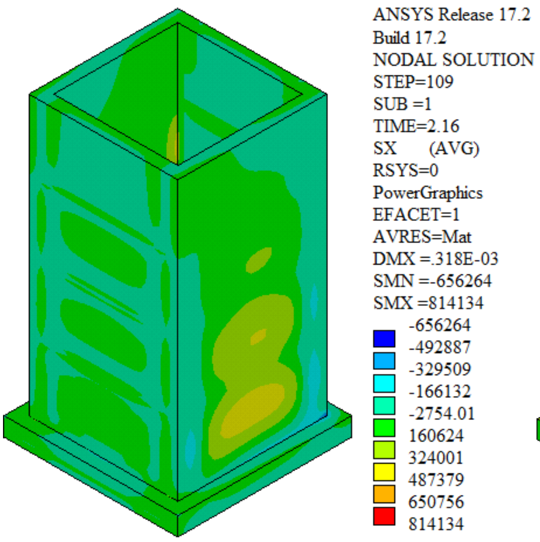

(c) Non-isolated structure with triple baffles

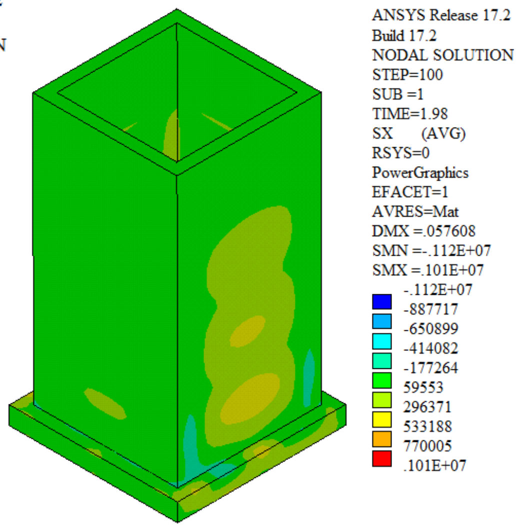

(d) Isolated structure with triple baffles

Figure (9): Wall stress under the action of El-Centro waves (PGA=0.4g)

As shown in Fig. 9, the nephogram distribution of the wall plate is changed greatly due to the introduction of the baffle, where there are more stress extremum regions. For the non-isolated and isolated structures with triple baffles, the maximum stresses are reduced by 47% and 26%, respectively, compared to the corresponding structures with double baffles. For the isolated structures with double and triple baffles, the maximum stresses are reduced by 11% and -20%, respectively, compared to the corresponding non-isolated structures. Thus, it can be seen that the number of baffles has a significant influence on the stress distribution and peak value of the wall plate. In addition, the isolation also has a certain effect on the distribution of the wall stress.

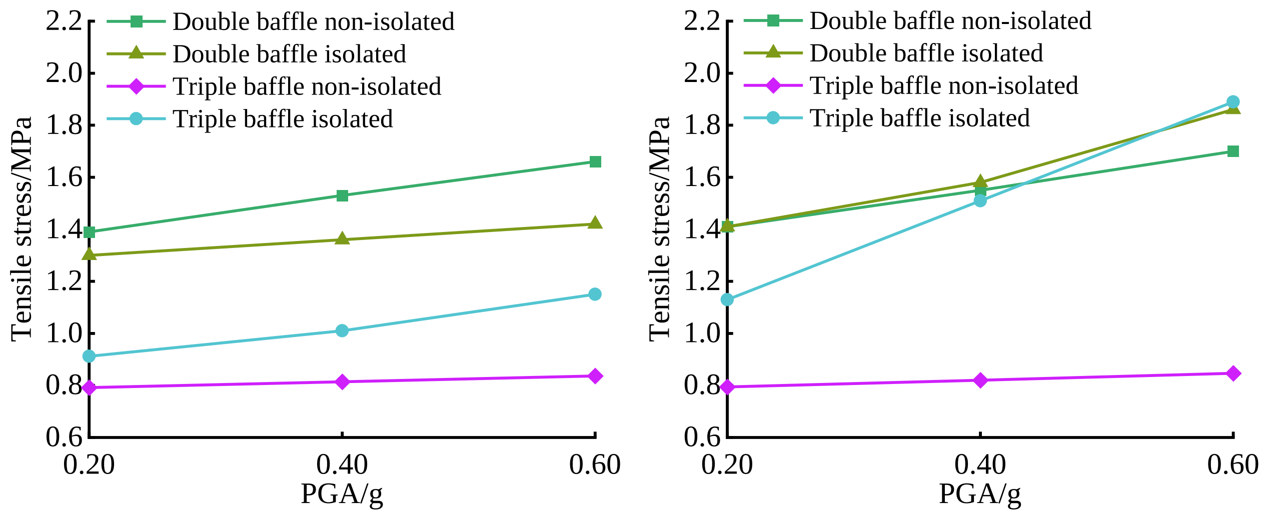

(a) El-Centro waves (b) Tianjin waves

Figure (10): Wall tensile stress

According to Fig. 10, under the action of El-Centro waves, for the tensile stress of the wall plate, the non-isolated structure with triple baffles < the isolated structure with triple baffles < the isolated structure with double baffles < the non-isolated structure with double baffles. Under the action of Tianjin waves, the tensile stress of the wall plate corresponding to the non-isolated structure with triple baffles is obviously smaller than that of the other three cases. Under the action of El-Centro waves, the rubber isolation reduces the tensile stress of the wall plate of the structure with double baffles, but it does not exert a shock absorption effect on the tensile stress of the structure with triple baffles.

The number of baffles has a very obvious effect on the damping control effect of the tensile stress of the wall plate. Under the action of El-Centro waves, when PGA is 0.2g, the wall plate tensile stresses of non-isolated structures with double baffles and triple baffles are 1.39MPa and 0.79MPa, which are reduced by 43%. When PGA is 0.4 g, the wall plate tensile stress of non-isolated structures with double baffles and triple baffles are 1.53MPa and 0.81MPa, which are reduced by 47%. When the PGA is 0.6g, the wall plate tensile stresses of non-isolated structures with double baffles and triple baffles are 1.66MPa and 0.84MPa, which are reduced by 49%. Under the action of Tianjin waves, when PGA is 0.2g, the wall plate tensile stresses of non-isolated structures with double baffles and triple baffles are 1.41MPa and 0.79MPa, which are reduced by 44%. When the PGA is 0.4 g, the wall plate tensile stresses of non-isolated structures with double baffles and triple baffles are 1.55MPa and 0.82MPa, which are reduced by 47%. When PGA is 0.6g, the wall plate tensile stresses of non-isolated structures with double baffles and triple baffles are 1.70MPa and 0.85MPa, which are reduced by 50%. Under the action of Tianjin waves, when PGA is 0.6g, the wall tensile stresses of the isolated structures with double and triple baffles are increased by 10% and 122%, respectively, compared to those of the non-isolated structures.

Whether under the action of near-field seismic waves (El-Centro waves) or far-field seismic waves (Tianjin waves), with the increase of PGA, the tensile stress of the non-isolated liquid storage structure with triple baffles remains basically unchanged. The rubber isolation reduces the tensile stress of the structure with double baffles under the action of El-Centro waves, but increases the stress of the structure with triple baffles. Under the action of Tianjin waves, the rubber isolation has an amplifying effect on the tensile stress of both structures with double baffles and triple baffles, but the amplifying effect on the structure with triple baffles is more significant. This may be due to the fact that the rubber isolation increases the structural sway, but the baffles impede the fluid sway, thus creating more stress. Thus, it can be seen that when the baffles reach a certain number, their strengthening effect on the structure will be more significant. Through the reasonable arrangement of horizontal baffles, the seismic capacity of concrete rectangular liquid storage structure with large height-width ratio can be effectively improved.

(2) Baffle stress

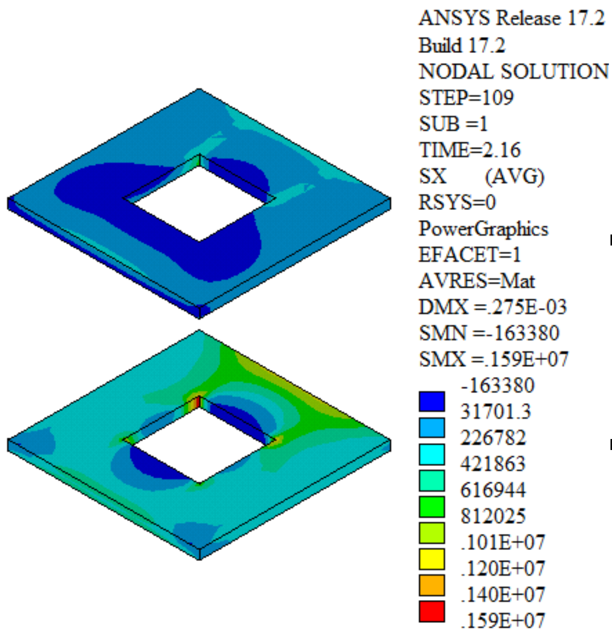

(a) Non-isolated structure with double baffles

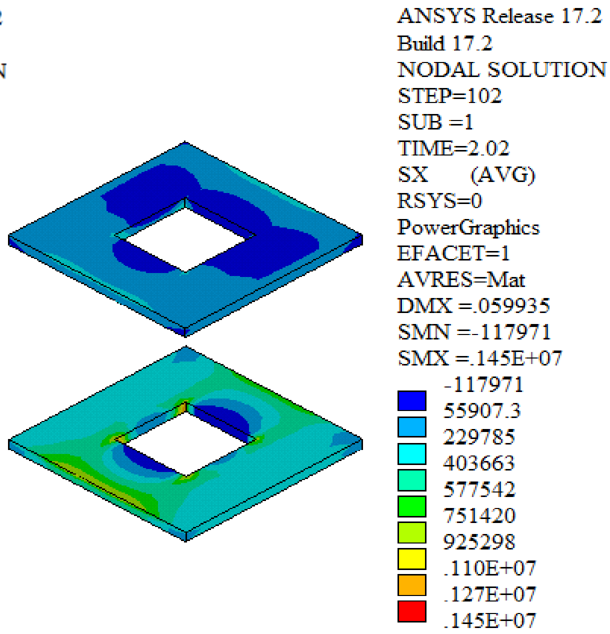

(b) Isolated structure with double baffles

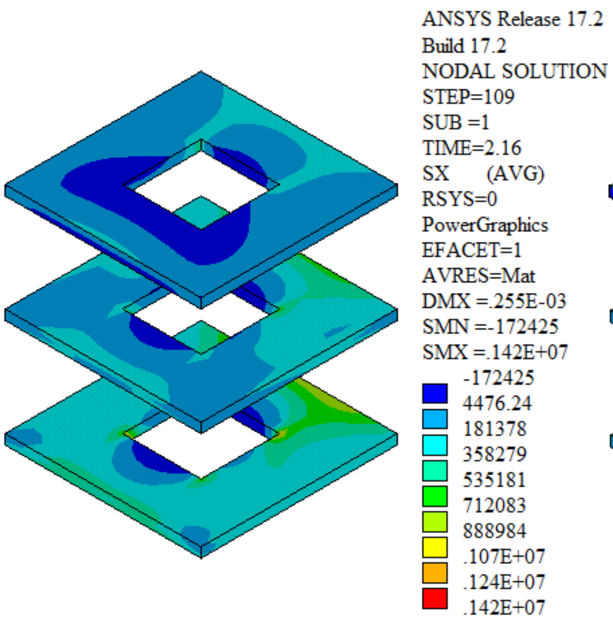

(c) Non-isolated structure with triple baffles

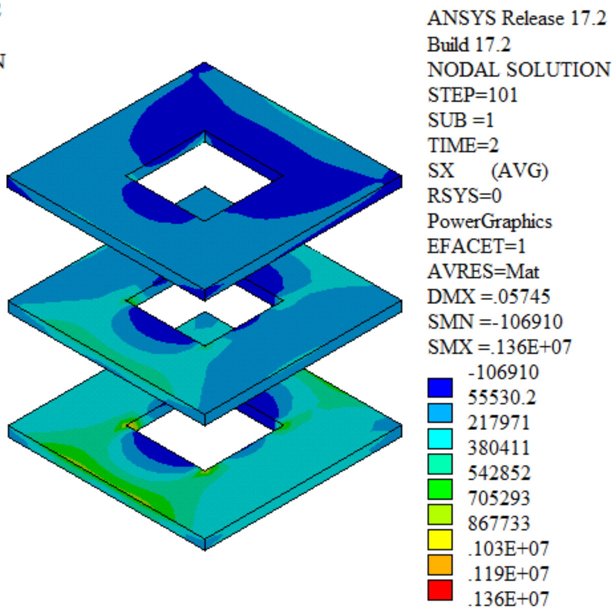

(d) Isolated structure with triple baffles

Figure (11): Baffle stress under the action of El-Centro waves (PGA=0.4g)

According to Fig. 11, the maximum baffle stresses of the non-isolated structures with triple baffles and double baffles are 1.42 MPa and 1.59 MPa, respectively. It is shown that the baffle stress is reduced by 11.0% when the number of baffles is increased from 2 to 3. The maximum baffle stresses of the isolated structures with triple baffles and double baffles are 1.36 MPa and 1.45 MPa, respectively, which are reduced by 4% and 9% compared to those of the corresponding non-isolated structure. It can be seen that a reasonable increase in the number of baffles has a significant effect on reducing the baffle stress and the isolation has a certain damping effect on the baffle stress.

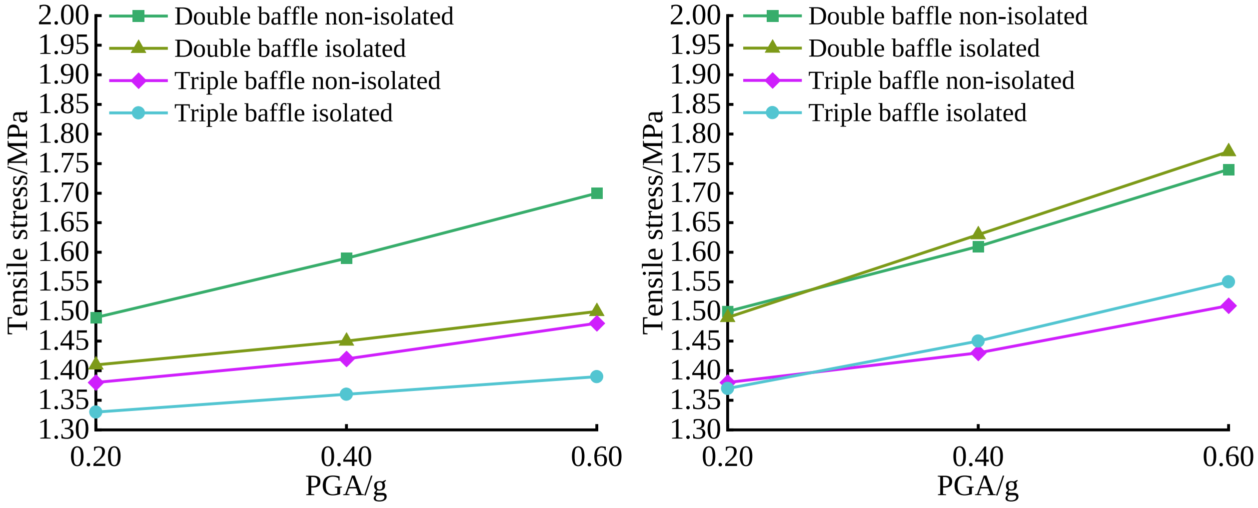

(a) El-Centro waves (b) Tianjin waves

Figure (12): Tensile stress of horizontal baffles

It is shown from Fig. 12 that under the action of El-Centro waves and Tianjin waves, the tensile stress of the baffles shows different laws with the increase of PGA. For the baffle tensile stress, under the action of El-Centro waves, the isolated structure with triple baffles < the non-isolated structure with triple baffles < the isolated structure with double baffles < the non-isolated structure with double baffles. Under the action of Tianjin waves, when PGA is 0.4g and 0.6g, the isolation has no effect on the baffle tensile stress.

In conclusion, the number of baffles has a significant effect on controlling the baffle stresses under both far-field seismic waves and near-field seismic waves. The isolation only has a certain damping effect on the baffle tensile stress under the action of near-field seismic waves, while under the action of far-field seismic waves, the damping effect of the isolation on the baffle tensile stress is not significant.

Liquid Sloshing Wave Height

Due to space limitations, taking El-Centro waves (PAG=0.4g) as an example, the liquid sloshing wave height is shown in Fig. 13. The calculated results of the liquid sloshing wave height corresponding to PGA of 0.2g, 0.4g and 0.6g are shown in Table 1.

Table 1. Maximum liquid sloshing wave height (unit: m)

Seismic waves	**El-Centro waves**			**Tianjin waves**		
Structure type	**PGA**					
	0.2g	**0.4g**	**0.6g**	**0.2g**	**0.4g**	**0.6g**
Non-isolated structure with double baffles	0.206	0.413	0.620	0.247	0.495	0.743
Isolated structure with double baffles	0.237	0.513	0.789	0.279	0.596	0.921
Non-isolated structure with triple baffles	0.206	0.413	0.620	0.247	0.495	0.743
Isolated structure with triple baffles	0.238	0.514	0.791	0.278	0.595	0.918

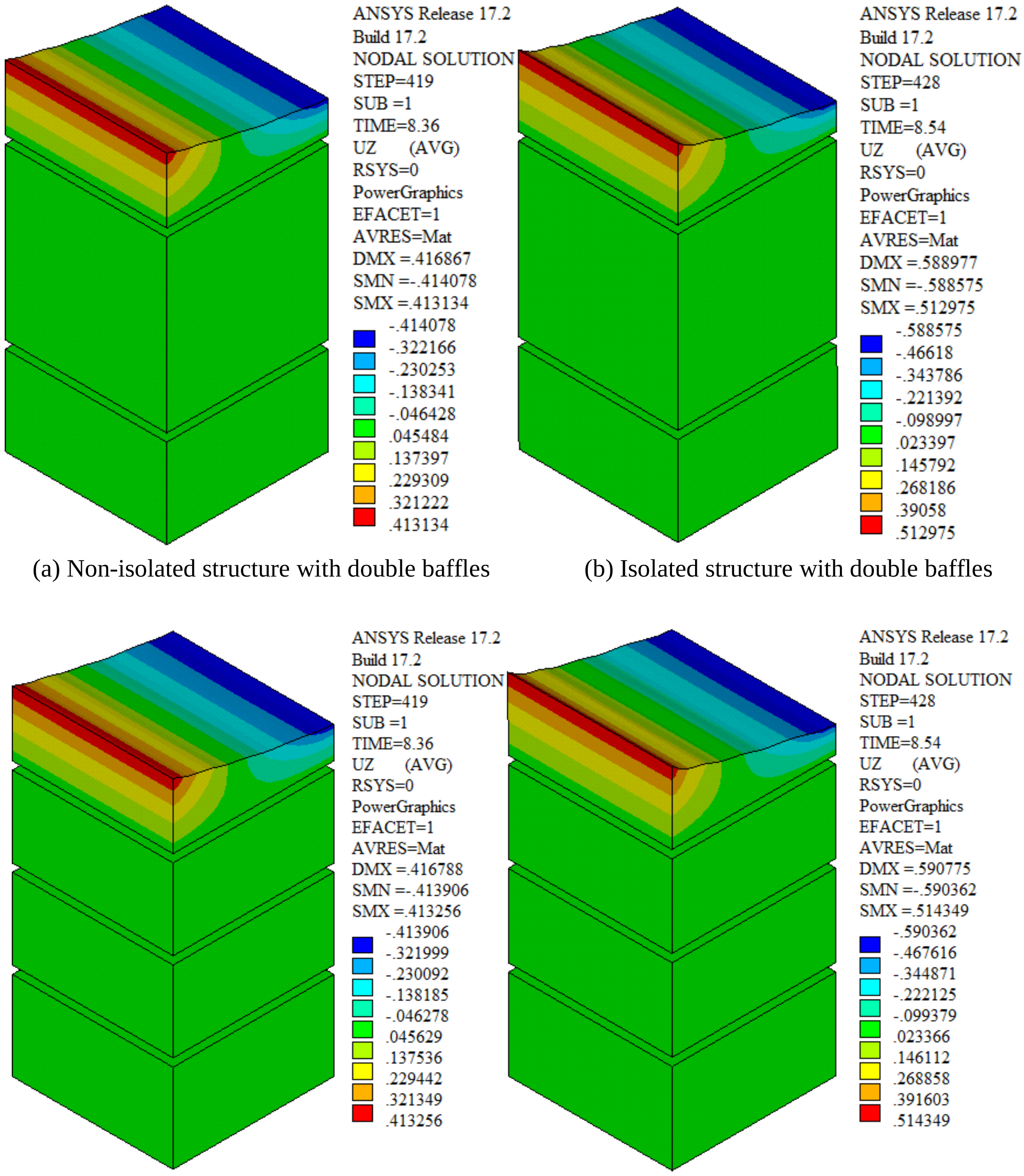

(a) Non-isolated structure with double baffles (b) Isolated structure with double baffles

(c) Non-isolated structure with triple baffles (d) Isolated structure with triple baffles

Figure (13): Maximum liquid sloshing wave height under the action of El-Centro waves (PGA=0.4g)

As shown in Fig. 13, under the action of El-Centro waves, the maximum liquid sloshing waves height of the isolation structure is increased by about 25% compared to that of the non-isolated structure, while the maximum liquid sloshing waves height of the structures with triple baffles does not change significantly compared to structures with double baffles.

As can be seen, the maximum liquid sloshing wave heights corresponding to the non-isolated structure with double baffles and the non-isolated structure with triple baffles are the same. In addition, the sloshing wave heights of the isolated structure with double baffles and the isolated structure with triple baffles are very close. The main reason is that in the case of double baffles and triple baffles, the uppermost baffle is at the same position. Therefore, increasing the number of baffles or isolation is not effective in controlling the maximum liquid shaking wave height of the structure.

CONCLUSIONS

Concrete rectangular liquid storage structure with large height-width ratio has good application prospects due to saving land resources. With the increase of liquid storage height, the dynamic response of the structure under seismic action increases and the damage risk under the seismic action also increases. The effects of baffles and isolation on the dynamic responses of the structure are investigated. Near-field seismic waves and far-field seismic waves are selected to more accurately assess the effects of earthquakes on the structure. The main conclusions drawn are as follows:

(1) The structure with triple baffles is effective in reducing the wall tensile stresses (43%-50%) under both far-field seismic waves and near-field seismic waves, while the baffle number has a significant influence on the wall tensile stress. and reasonable arrangement of baffles can effectively reduce the probability of wall cracking.

(2) The structure with triple baffles has a significant effect on controlling the tensile stresses of the horizontal baffle. When PGA is 0.4g, under the action of El-Centro waves, compared to the non-isolated structure with double baffles, the tensile stress of the horizontal baffle of the non-isolated structure with triple baffles is decreased by 11%. Therefore, increasing the number of baffles helps reduce the probability of baffle cracking.

(3) Rubber isolation amplifies the liquid shaking wave height by approximately 25% and does not significantly reduce the wall plate tensile stress and baffle stress. Namely, rubber isolation cannot play a good damping role in the control of dynamic responses of the concrete rectangular liquid storage structure with large height-width ratio.

Acknowledgements

This paper is a part of the National Natural Science Foundation of China (Grant number: 52168071, 51908267) and a part of the Gansu Province Higher Education Innovation Fund Project (Grant No. 2023-027).

Appendix A

Some of the important equations are as follows:

Volumetric strain ε_v can be expressed as:

$$\varepsilon_v = \frac{\partial u_{fx}}{\partial x} + \frac{\partial u_{fy}}{\partial y} + \frac{\partial u_{fz}}{\partial z}. \tag{1A}$$

The free surface stiffness matrix $\mathbf{S}_f$, stiffness of the liquid matrices $\mathbf{K}_f$ and mass matrices of the liquid $\mathbf{M}_f$ can be expressed as:

$$\begin{cases} \boldsymbol{K}_f = \sum \boldsymbol{K}_f^e, \boldsymbol{K}_f^e = \int_V \boldsymbol{B}_f^{eT} \boldsymbol{C}_f \boldsymbol{B}_f^e dV_e \\ \boldsymbol{S}_f = \sum \boldsymbol{S}_f^e, \boldsymbol{S}_f^e = \rho_f g \int_V \boldsymbol{h}_f^T \boldsymbol{h}_s dA^e \\ \boldsymbol{M}_f = \sum \boldsymbol{M}_f^e, \boldsymbol{M}_f^e = \rho_f \int_V \boldsymbol{H}_f^T \boldsymbol{H} dV^e \end{cases} \tag{2A}$$

The form of the damping matrix **C** is as follows:

$$\boldsymbol{C} = \sum_{j=1}^{N} \beta_j \boldsymbol{K} \tag{3A}$$

where β_j denotes the stiffness matrix multiplier for material *j*.

Table A1. Materials and elements for the model

Materials	Element Types	Material property		
		Multi-linear Isotropic		
		Points	**Strain**	**Stress (MPa)**
		1	0.0002	5.092
		2	0.0004	9.648
		3	0.0006	13.668
		4	0.0008	17.152
		5	0.0010	20.100
Concrete	Solid 65	6	0.0012	22.512
		7	0.0014	24.388
		8	0.0016	25.728
		9	0.0018	26.532
		10	0.0020	26.800
		11	0.0033	26.800
		Poisson's ratio	0.2	
		Density	2500kg/m^3	

Water	Fluid 80	**Linear Isotropic**	
		Bulk modulus	2100MPa
		Density	1000kg/m^3
Rubber	Solid 185	**Mooney-Rivlin**	
		C_{10}	1.20MPa
		C_{01}	-0.35MPa
		Poisson's ratio	0.499
		Density	850kg/m^3

Symbols

ρ_f	Liquid density
v_f	Liquid velocity
$\bar{v}_f$	Coordinate system velocity
τ_f	Liquid stress tensor
f^B	External force vector acting on the liquid
E	Specific internal energy
D	Strain rate tensor
$\boldsymbol{n}$	Normal vector on the contact surface
u_s	Structure displacements on the contact surface
u_f	Liquid displacements on the contact surface
v_s	Structure velocity
a_s	Structure acceleration
a_f	Liquid acceleration
I	Contact surface
P	Liquid pressure
C_{11}	Bulk modulus
C_{22}, C_{33}, C_{44}	Constraint parameters
P_x, P_y, P_z	Rotational stresses
w_x, w_y, w_z	Rotations about the Cartesian axes *x*, *y* and *z*
u_{fx}, u_{fy}, u_{fz}	Displacement components of liquid in *the x*, *y* and *z* directions
ε_v	Volumetric strain
$\mathbf{S}_f$	Free surface stiffness matrix
$\mathbf{u}_{fs}$	Free surface vertical displacement vector
$\mathbf{K}_f$	Stiffness matrices of the liquid
$\mathbf{M}_f$	Mass matrices of the liquid
$\boldsymbol{P}^e$	Pressure along the element interface
$\boldsymbol{u}_n^e$	Displacement along the element interface
$\boldsymbol{f}_e$	Force acting on the element
$\boldsymbol{\delta}$	Element displacement
f_x, f_y, f_z	Node forces in *the x*, *y* and *z* directions
u, v, w	Node displacements in the *x*, *y* and *z* directions
e	Element on the interaction boundary
$\mathbf{M}_s$, $\mathbf{C}_s$, $\mathbf{K}_s$	Positive definite n×n order mass, damping and stiffness matrices
$\boldsymbol{u}_s(t)$, $\dot{\boldsymbol{u}}_s(t)$, $\dot{\boldsymbol{u}}_s(t)$	Displacement, velocity and acceleration of the coupled system
$\ddot{\boldsymbol{u}}_g(t)$	Earthquake acceleration vector
$\boldsymbol{Q}$	Fluid-structure coupling matrix
$\boldsymbol{P}$	Hydrodynamic pressure

C_{10}, C_{01}	Material constants generally determined by the experiment
I_1, I_2	The first and the second invariants of the deviatoric component of the Cauchy Green deformation tensor
D_1	Incompressibility coefficient
J	Ratio of the deformed volume to the undeformed volume.

REFERENCES

Avval, I.T. (2012). "Dynamic response of concrete rectangular liquid tanks in three-dimensional space". Theses and Dissertations.

Cai, C., Zheng, H., Khan, M.S., and Hung, K.C. (2002, April). "Modeling of material damping properties in ANSYS". CADFEM Users' Meeting & ANSYS Conference, 9-11.

Cheng, X.S., Jing, W., and Gong, L.J. (2019). "Liquid sloshing problem in a concrete rectangular LSS with a vertical baffle". Arabian Journal for Science and Engineering, 44, 4245-4256.

Cheng, X.S., Liu, B., Cao, L.L., Yu, D.P., and Feng, H. (2018). "Dynamic response of a base-isolated CRLSS with baffle". Structural Engineering and Mechanics: An International Journal, 66 (3), 411-421.

Hajimehrabi, H., Behnamfar, F., Samani, A.K., and Goudarzi, M. A. (2019). "Fragility curves for baffled concrete cylindrical liquid-storage tanks". Soil Dynamics and Earthquake Engineering, 119, 187-195.

Hosseini, M., Goudarzi, M. A., and Soroor, A. (2017). "Reduction of seismic sloshing in floating roof liquid storage tanks by using a suspended annular baffle (SAB)". Journal of Fluids and Structures, 71, 40-55.

Huang, J.L., Xie, G.J., and Liu, Z.W. (2008). "Finite element analysis of super-elastic rubber materials based on the Mooney-Rivlin and Yeoh model". China Rubber/Plastics Technology and Equipment, 34 (12), 22-26.

Jin, H., Calabrese, A., and Liu, Y. (2021). "Effects of different damping baffle configurations on the dynamic response of a liquid tank under seismic excitation". Engineering Structures, 229, 111652.

Luo, H., Zhang, R.F., and Weng, D.G. (2016). "Mitigation of liquid sloshing in storage tanks by using a hybrid control method". Soil Dynamics and Earthquake Engineering, 90, 183-195.

Nikoomanesh, M.R., Moeini, M., and Goudarzi, M.A. (2019). "An innovative isolation system for improving the seismic behaviour of liquid storage tanks". International Journal of Pressure Vessels and Piping, 173, 1-10.

Rawat, A., and Matsagar, V. (2022). "An oblate spheroid base isolator and floating surface diaphragm for seismic protection of liquid storage tanks". Journal of Earthquake Engineering, 26 (10), 5447-5475.

Rawat, A., Matsagar, V.A., and Nagpal, A.K. (2019). "Numerical study of base-isolated cylindrical liquid storage tanks using coupled acoustic-structural approach". Soil Dynamics and Earthquake Engineering, 119, 196-219.

Safari, S., and Tarinejad, R. (2018). "Parametric study of stochastic seismic responses of base-isolated liquid storage tanks under near-fault and far-fault ground motions". Journal of Vibration and Control, 24 (24), 5747-5764.

Saha, S.K., Sepahvand, K., Matsagar, V.A., Jain, A.K., and Marburg, S. (2016). "Fragility analysis of base-isolated liquid storage tanks under random sinusoidal base excitation using generalized polynomial chaos expansion–based simulation". Journal of Structural Engineering, 142 (10), 1-12.

Shaker, Q.M., and Kamonna, H.H. (2016). "Non-linear analysis of reinforced concrete beams strengthened by prestressed CFRP sheets under static loads". Jordan Journal of Civil Engineering, 10 (1), 93-106.

Shakir, Q.M. (2016). "Non-linear analysis of high strength reinforced concrete beams with large openings". Jordan Journal of Civil Engineering, 10 (4), 451-461.

Shakir, Q.M., and Abdlsaheb, S.D. (2022). "Rehabilitation of partially damaged high strength RC corbels by EB FRP composites and NSM steel bars". In: Structures, 38, 652-671.

Shakir, Q.M., and Hamad, S.A. (2021). "Behavior of pocket-type high-strength RC beams without or with dapped ends". Practice Periodical on Structural Design and Construction, 26 (4), 1-12.

Shakir, Q.M., Al-Sahlawi, Y.M., Abd, B.B., and Hamad, S.A. (2023). "Non-linear finite element analysis of high-strength reinforced concrete beams with severely disturbed regions". Jordan Journal of Civil Engineering, 17 (1), 22-33.

Shekari, M.R., Hekmatzadeh, A.A., and Amiri, S. M. (2019). "On the non-linear dynamic analysis of base-isolated three-dimensional rectangular thin-walled steel tanks equipped with vertical baffles". Thin-walled Structures, 138, 79-94.

Sun, Y., Zhou, D., Amabili, M., Wang, J.D., and Han, H.X. (2020). "Liquid sloshing in a rigid cylindrical tank equipped with a rigid annular baffle and on soil foundation". International Journal of Structural Stability and Dynamics, 20 (03), 2050030.

Sussman, T., and Bathe, K.J. (1987). "A finite element formulation for non-linear incompressible elastic and inelastic analysis". Computers & Structures, 26 (1-2), 357-409.

Tang, Z.Y., Hong, Y., He, L.S, and Li, Z.B. (2021). "Seismic performance of storage tank isolated by different isolators through real-time hybrid simulation". International Journal of Structural Stability and Dynamics, 21 (13), 1-20.

Zang, Q.S., Fang, H.Y., Liu, J., and Lin, G. (2019). "Boundary element model for investigation of the effects of various porous baffles on liquid sloshing in the two dimensional rectangular tank". Engineering Analysis with Boundary Elements, 108, 484-500.